Chemical Engineering Journal 530 (2026) 172982

Contents lists available at ScienceDirect

Chemical Engineering Journal

journal homepage: www.elsevier.com/locate/cej

Influence of H_2:CO_2 ratio and low CO supplementation on product distribution and carboxylate reduction in *Clostridium autoethanogenum*

Andrés Suazo [a,b], Ivette Parera Olm [b], Fabián Otálora [a], Jimmy Martínez-Ruano [a,c], Raúl Conejeros [a], Germán Aroca [a], Diana Z. Sousa [b,*]

[a] Escuela de Ingeniería Bioquímica, Pontificia Universidad Católica de Valparaíso, Valparaíso, Chile
[b] Laboratory of Microbiology, Wageningen University & Research, Wageningen, The Netherlands
[c] Department of Chemical Engineering, Universidad de la Frontera, Temuco, Chile

ARTICLE INFO

Keywords:
Acetogen
Gas fermentation
Carboxylic acids
Alcohols
FBA

ABSTRACT

Gas fermentation using H_2:CO_2 and CO as feedstocks offers a sustainable alternative to fossil fuel-derived production of chemicals. *Clostridium autoethanogenum* is an industrially relevant acetogen for this process, but the effects of gas compositions — particularly H_2:CO_2 ratios — on product distribution are still unclear, hindering optimisation. Previous studies have not provided comprehensive analysis of metabolic responses during the coutilisation of multiple gaseous substrates in batch cultures. This study investigates how H_2:CO_2 ratios and low-level CO supplementation steer *C. autoethanogenum* metabolism, specifically influencing acetogenic and solventogenic pathways (acetate and ethanol production) and exogenous carboxylate reduction (conversion of butyrate to butanol). Batch cultures were conducted with H_2:CO_2 ratios of 1:1, 2.5:1, and 4:1, CO supplementation of 0%, 2%, and 5%, and butyrate addition of 0, 10, and 20 mM. Substrate consumption, product generation, and biomass were monitored over time. Flux balance analysis (FBA) was employed to estimate the changes in internal fluxes during different stages of the culture. Ethanol production positively correlated with initial H_2:CO_2 ratios, increasing from 0.7 mM ± 0.6 mM at 1:1 to 6.0 mM ±1.8 mM at 4:1. Acetate concentrations remained stable at 24.7 mM ± 4.7 mM. Higher initial CO pressures boosted biomass and CO uptake rates. Butyrate addition accelerated butanol but delayed ethanol production, indicating competition for reducing equivalents. Overall, this study demonstrates how H_2:CO_2:CO ratios can be strategically adjusted to steer *C. autoethanogenum* metabolism. The combination of factorial and Box–Behnken experimental design provided a flexible approach to generate data that can guide gas fermentation strategies towards targeted chemical production.

1. Introduction

Microbial fermentation of H_2/CO_2 and CO-rich gases offers a sustainable route for transforming residual carbon into fuels and chemicals, aligning with circular economy principles [1]. Feedstocks include industrial flue gases, such as steel mill off-gas, and syngas from gasification of lignocellulosic residues and organic waste. CO-rich flue gases differ from syngas streams, which have variable CO:CO_2:H_2 ratios [2]. Acetogenic bacteria drive the gas fermentation process through the Wood–Ljungdahl Pathway (WLP), fixing CO_2 and CO into acetyl-CoA for biomass growth, producing acetate and ethanol as main end products [3]. CO_2-rich streams require an electron donor such as H_2, while CO can serve as both carbon and energy source [4]. Gas-fermentation pathways can reduce GHG emissions by 67%–98% relative to petrochemical ethanol production; furthermore, compared with biomass-derived ethanol, gas fermentation still offers substantially lower emissions, with 4 to 10 fold reductions when using the same feedstock [5]. Among acetogens, *Clostridium autoethanogenum* has emerged as a model industrial strain due to its robust metabolism and scalability [6], making it an attractive chassis for targeted product formation. The central metabolism of *C. autoethanogenum* is illustrated in Fig. 1.

Industrial gas fermentation remains primarily focused on ethanol as the main product, though extending product ranges to C_{4+} alcohols and acids is a major research focus [12]. Monocultures of acetogens like *C. carboxidivorans* can reach combined C_{4+} selectivities of 64% in microbial electrosynthesis and 31% in batch fermentation [13–15], but ethanol or acetate typically remains as the predominant fermentation

* Corresponding author.
E-mail addresses: fabian.otalora.t@mail.pucv.cl (F. Otálora), diana.sousa@wur.nl (D.Z. Sousa).

https://doi.org/10.1016/j.cej.2026.172982
Received 17 October 2025; Received in revised form 21 December 2025; Accepted 12 January 2026
Available online 17 January 2026

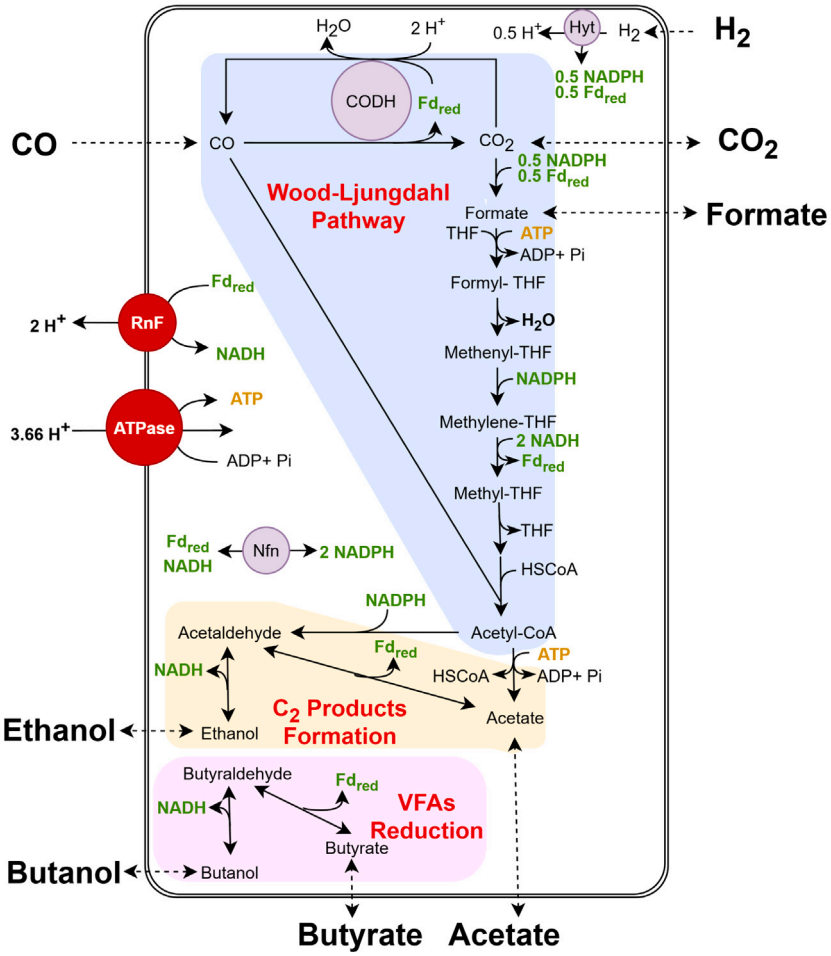

Fig. 1. Simplified scheme of *C. autoethanogenum* central metabolism illustrating the Wood–Ljungdahl Pathway, C_2 product formation (ethanol and acetate) and butyrate to butanol reduction (adapted from Mock et al. [7]; Isom et al. [8]; [9]; Allaart et al. [10] & Diender et al. [11]). For simplicity, only the reduced form of each redox carrier is shown.

product. Cocultures with chain elongators such as *C. kluyveri* can be used for product diversification, converting acetate and ethanol into butyrate, caproate, and corresponding alcohols [9,16–21]. These systems achieve combined C_{4+} selectivities of 39%–56%, though acetate often remains at 43%–58%. Exogenous acetate or ethanol supplementation can improve C_{4+} yields by reducing competition for C_2 intermediates and driving volatile fatty acid reduction pathways [16,17].

Butanol stands out among C_{4+} products for its higher energy density and compatibility with existing fuel infrastructure [22]. Two strategies have shown promise for improving butanol selectivity in gas-fermenting cocultures: (i) increasing electron donor supply (CO or H_2) favours the reduction of butyrate to butanol while limiting further chain-elongation [23]. Reduction of butyrate to butanol has been shown in monocultures of *C. ljungdahlii*, *C. ragsdalei* and cocultures of *C. autoethanogenum* with *C. kluyveri* adding exogenous carboxylates and partial CO pressures (p_{CO}) above 1 bar [8,17,24]. (ii) maintaining an ethanol-to-acetate (E:A) ratio below 1:1 in cocultures promotes butyrate accumulation over caproate, increasing precursor availability for butanol [25,26]. These strategies highlight the potential for targeted manipulation of gas composition and metabolite ratios to drive desirable product pathways.

Gas composition and ratios directly affect carbon fixation efficiency and product distribution. In *C. autoethanogenum* chemostat cultures grown on H_2:CO_2, adding 2% CO increased ethanol concentrations from 2.4 ± 0.3 to 9.7 ± 0.4 g L^{-1} and boosted carbon distribution to ethanol from 54 ± 3 to 66 ± 2 C-mol%, while raising CO_2 uptake rates from 460 ± 80 to 540 ± 20 mmol $gCDW^{-1}$ d^{-1} [27]. In *C. ljungdahlii*, an H_2:CO ratio of 2:1 promotes acetate production (E:A produced = 0.7) after CO depletion, whereas a 0.5 ratio yields an E:A of 1.1, diverting carbon towards CO_2 and 2,3-butanediol [28]. Cocultures of *C. autoethanogenum* and *C. kluyveri* with 80% H_2 and 20% CO_2 enhanced butyrate yields, though at lower production rates than H_2:CO mixtures, likely due to near-1:1 E:A ratios in monocultures under identical conditions [17,29,30]. Reducing CO levels can improve the selectivity of acetate/ethanol and alleviate toxicity, thus stabilising monoculture and coculture performance [31,32], indicating that CO supply must be precisely tuned to balance carbon fixation efficiency with targeted product formation.

Despite advances in gas fermentation, a critical gap remains in understanding *C. autoethano-genum*'s solventogenic pathways at low CO concentrations. Most carboxylate reduction studies in acetogens have used high CO levels (>40%), which lower carbon fixation efficiency and favour byproducts such as lactate and butanediol [31]. This observation aligns with the approach of optimising syngas composition to shift redox balance and precursor availability in ways that strongly influence butyrate reduction to butanol. Addressing this gap requires systematic experimentation across a range of H_2:CO_2 ratios, CO levels, and carboxylate concentrations [33]. Such integrated studies would help identifying multiple substrate effect in *C. autoethanogenum* metabolism to better understand carboxylate reduction pathways and identify optimal bioprocess conditions for targeted product formation.

The present study investigates the effect of varying initial H_2:CO_2 ratios, CO supplementation and butyrate concentration on the ethanol:acetate ratio and solventogenic metabolism in batch cultures

of *C. autoethanogenum*. To fully explore the relationship between gas composition and metabolic behaviour while optimising the experimental workflow, a statistical design of experiments (DoE) approach was employed, establishing correlations between the inputs (substrates) and metabolic responses [34]. The Box–Behnken design, particularly effective for three-factor studies, was used here, as it offers higher efficiency over full factorial or central composite designs and supports predictive modelling of fermentation performance parameters across a defined experimental space [35,36]. The DoE framework thus provides empirical insights, that has the potential to guide the optimisation of monoculture and coculture strategies for the selective production of secondary alcohols, such as butanol, via gas fermentation.

2. Materials and methods

2.1. Microorganism and cultivation

C. autoethanogenum DSM 10061 was obtained from the German Collection of Microorganisms and Cell Cultures (DSMZ, Braunschweig, Germany). The ATCC 1754 medium was used for cultivation, with the following composition (per litre): 1 g NH_4Cl, 1 g NaCl, 0.2 g $MgSO_4 \cdot 7H_2O$, 0.1 g KH_2PO_4, 0.02 g $CaCl_2$ and 0.5 mg resazurin. The medium was supplemented with 1% v/v of a trace elements solution that contained (per litre): 20 mg of nitrilotriacetic acid (NTA), 10 mg $MnSO_4 \cdot H_2O$, 8 mg $Fe(SO_4)_2(NH_4)_2 \cdot 6H_2O$, 2 mg $CoCl_2 \cdot 6H_2O$, 2 mg $ZnSO_4 \cdot 7H_2O$, 0.2 mg $CuCl_2 \cdot 2H_2O$, 0.2 mg $NiCl_2 \cdot 6H_2O$, 0.2 mg $Na_2MoO_4 \cdot 2H_2O$, 0.2 mg Na_2SeO_4 and 0.2 mg $Na_2WO_4 \cdot 2H_2O$. The medium was boiled, and subsequently cooled on ice while bubbling N_2 before the addition of 0.75 g cysteine (per litre) as a reducing agent. The pH was adjusted to 6.0. The medium was dispensed into serum bottles that were immediately sealed with rubber stoppers and aluminium caps. The headspace of the bottles was gas-exchanged with nitrogen. The bottles were autoclaved immediately after preparation. Before inoculation, the medium was further supplemented with yeast extract (0.25 g L^{-1}) and a vitamin solution at a 1:100 dilution containing (per litre): 2 mg biotin, 2 mg folic acid, 10 mg pyridoxine-HCl, 10 mg thiamine-HCl, 5 mg riboflavin, 5 mg nicotinic acid, 5 mg calcium pantothenate, 5 mg cyanocobalamine, 5 mg p-aminobenzoic acid and 5 mg lipoic acid. When specified (Runs 10–18, Table 1), butyrate was supplemented from a sterile 1 M stock solution. For culture propagation, 1.5 bar CO was used as substrate. Cultivation was performed at 37 °C with shaking at 150 rpm.

2.2. Experimental design

The effect of gas composition on *C. autoethanogenum* metabolism was investigated following a phased experimental design approach. Initially, a two-factor, three-level factorial design was considered to evaluate the impact of initial p_{CO} and H_2:CO_2 ratio (Runs 1–9, Table 1). The central point of this design was set at an initial CO supplementation of 5% (0.075 bar) and an H_2:CO_2 ratio of 2.5 (corresponding to 64.3% H_2 and 25.7% CO_2 in the gas mixture, see Table 1).

Subsequently, a Box–Behnken design was applied to comprehensively assess the influence of three independent variables: initial p_{CO}, H_2:CO_2 ratio, and initial butyrate concentration. The levels for initial p_{CO} and H_2:CO_2 ratio were maintained from the preliminary factorial design (Runs 6–18, Table 1). For butyrate concentration, a central level of 10 mM was selected, based on concentrations used in previous studies Perez et al. [24] . The level +1 for added CO and butyrate was defined by doubling the central point value, while the level −1 corresponded to the absence of the compound. However, for the H_2:CO_2 ratio, the "+1" and "−1" levels were established by incrementing or decrementing the central point ratio by 1.5 units, respectively. This approach ensured the presence of H_2 in all cultures, establishing different levels where either CO_2 or H_2 would become limiting factors for carbon fixation. The specific values for each experimental run are detailed in Table 1.

2.3. Batch bottle experiments

The experimental design described above was executed in two batch experiments, conducted in 250-mL serum bottles with 50-mL medium as described above and variable headspace composition. The first experiment was aimed at evaluating the effect of different H_2:CO_2 ratios and CO supplementation on the physiology of *C. autoethanogenum*. For this, the headspace of bottles was pressurised to 1.5 bar with the corresponding mixture of H_2, CO_2, CO and N_2, as detailed in Table 1. The second experiment aimed at assessing butyrate reduction by *C. autoethanogenum* under different H_2:CO_2 mixtures and CO supplementation, as detailed in Table 1. All bottles were inoculated (5% v/v) with an exponentially growing culture of *C. autoethanogenum*, and incubated at 37 °C with agitation (150 rpm). Liquid (1 mL) and headspace (0.2 mL) samples were routinely collected during 7 days for further analysis. pH was monitored at each sampling point for the duration of the cultures. All conditions were tested in triplicate, with results expressed as mean ± standard deviations. To assess for statistically significant differences between the means of the three levels of each factor, a one-way ANOVA was performed using the open-source statistical package Pingouin in Python 3. Results were considered statistically significant at $p < 0.01$.

2.4. Analytical methods

Cell dry weight (CDW) was determined by collecting 8 mL of culture at the end of cultivation. Cells were harvested by centrifugation and washed twice with distilled water containing 2.5 mM NaCl. The washed cell pellets were then transferred to pre-weighed aluminium foil dishes and dried at 105 °C until constant weight. A calibration curve was established by correlating dry weight measurements with optical density at 600 nm (OD_{600}). This calibration was subsequently used to estimate biomass concentration in batch cultures over time from OD_{600} readings.

Ethanol, acetate, formate, lactate, 2,3-butanediol, butyrate and butanol concentrations on the liquid phase were determined via high pressure liquid chromatography (HPLC; LC-2030C, Shimadzu). The HPLC was equipped with a MetaCarb 67H column (300 mm *x* 6.5 mm, Agilent Technologies) with UV and RI detectors for compound detection. The column was operated at 55 °C and 0.01 *N* H_2SO_4 was used as eluent at a flowrate of 1 mL min^{-1}. Gas phase composition was determined via gas chromatography (Compact GC 4.0, Global Analyser Solutions, The Netherlands). CO, H_2 and N_2 were measured using a Molsieve 5A column operated at 100 °C coupled to a Carboxen 1010 precolumn. CO_2 was measured using an Rt-Q-BOND column operated at 80 °C. In both channels, argon was used as carrier gas. Detection was performed in all cases via a thermal conductivity detector.

2.5. Parameter determination

Specific uptake and production rates were evaluated across three phases: exponential growth (period I), solvent production (period II), defined as a >20% increase in ethanol or butanol concentrations within 24 h, and post-CO depletion (period III). In cultures with no initial CO, period III rates were considered equivalent to those of solvent production (period II). Period II was defined as a relevant period of time to analyse flux distributions at the different observed production phases of the culture, which varied according to the gas composition used. Consequently, it could overlap with periods I or III whenever the solvent production criterion was fulfilled (e.g. Fig. 3). Specific time periods defined for each condition are shown in Supplementary File S1.

Specific growth rates (μ) were determined from the analytical solution of the mass balance Eq. (1), where X represents the biomass concentration.

Cell-specific uptake and production rates (q_k) were calculated from the mass balance equation (Eq. (2)), with C_k denoting the time-dependent concentration of extracellular component k (CO, CO_2, H_2,

Table 1
Coded and uncoded values for factorial (Runs 1–9) and Box–Behnken (Runs 6–18) experimental designs.

Run #	Coded Values			Uncoded Values			Headspace gas composition (% v/v)			
	x_1	x_2	x_3	X_1 H_2:CO_2	X_2 %CO	X_3 HBUT [mM]	H_2	CO_2	CO	N_2
1	1	1	−1	4	10	0	72.0	18.0	10.0	0.0
2	1	−1	−1	4	0	0	72.0	18.0	0.0	10.0
3	−1	−1	−1	1	0	0	45.0	45.0	0.0	10.0
4	−1	1	−1	1	10	0	45.0	45.0	10.0	0.0
5	0	0	−1	2.5	5	0	64.3	25.7	5.0	5.0
6	−1	0	−1	1	5	0	45.0	45.0	5.0	5.0
7	0	1	−1	2.5	10	0	64.3	25.7	10.0	0.0
8	0	−1	−1	2.5	0	0	64.3	25.7	0.0	10.0
9	1	0	−1	4	5	0	72.0	18.0	5.0	5.0
10	−1	−1	0	1	0	10	45.0	45.0	0.0	10.0
11	−1	1	0	1	10	10	45.0	45.0	10.0	0.0
12	0	0	0	2.5	5	10	64.3	25.7	5.0	5.0
13	1	−1	0	4	0	10	72.0	18.0	0.0	10.0
14	1	1	0	4	10	10	72.0	18.0	10.0	0.0
15	−1	0	1	1	5	20	45.0	45.0	5.0	5.0
16	0	−1	1	2.5	0	20	64.3	25.7	0.0	10.0
17	0	1	1	2.5	10	20	64.3	25.7	10.0	0.0
18	1	0	1	4	5	20	72.0	18.0	5.0	5.0

ethanol, acetate, formate, butyrate, butanol) over a defined interval from t_i to t_f.

$$\frac{dX}{dt} = \mu \cdot X \tag{1}$$

$$\frac{dC_k}{dt} = q_k \cdot X \tag{2}$$

For period I, q_k was calculated analytically as the coefficient of μ and the yield of the component relative to biomass (Y_{X/C_k}). For periods II and III, q_k was estimated using the integral viable cell concentration (IVCC, Eq. (4)), calculated by the trapezoidal rule [37,38]. Thus, q_k values were determined as shown in Eq. (3).

$$q_k = \begin{cases} \mu \left(\frac{C_{k_{t_f}} - C_{k_{t_i}}}{X_{t_f} - X_{t_i}} \right) & \text{Period I} \\ \frac{C_{k_{t_f}} - C_{k_{t_i}}}{IVCC} & \text{Periods II and III} \end{cases} \tag{3}$$

where:

$$IVCC = \int_{t_i}^{t_f} X dt \tag{4}$$

2.6. Response surface

Response surface equations were used to correlate the studied variables (H_2:CO_2 ratios, CO supplementation and butyrate addition) with substrate consumption, product concentration and q_i values obtained within the experimental design range. Multiple quadratic polynomial regression models were calculated for the set of parameters defined, according to Eq. (5) [39].

$$y = \beta_0 + \sum_{i=1}^{k} \beta_i x_i + \sum_{i=1}^{k} \beta_{ii} x_i^2 + \sum_{i=1}^{k-1} \sum_{j>i}^{k} \beta_{ij} x_i x_j \tag{5}$$

Where:

y : Response value.

x : Coded factor level value (as defined in Table 1).

β : Coefficients of the polynomial equation.

The method for determining the coefficients involves minimising the sum of squared errors (SSE) between the observed and predicted values. This minimisation is achieved through the application of the Sequential Least Squares Programming algorithm (SLSQP) using the optimisation tool minimize from the SciPy library in Python 3.

In instances where both the experimental results and the surface response equation suggested the presence of a local maximum within the investigated concentration range, constrained optimisation using the trust-region algorithm was employed. This approach facilitated the determination of the maximum response values through the response surface equation.

2.7. Flux balance analysis

Three published genome-scale models (GEMs)—iCLAU786 [40], MetaCLAU [31], and iHN637 [41]— were assessed to identify the most suitable metabolic network for representing the carbon flux distribution through flux balance analysis (FBA). LP optimisation was implemented in Python 3 using the GLPK solver interfaced via the COBRApy package [42]. To elucidate the competitive dynamics of acetate and butyrate reduction for shared reducing equivalents, butyrate reduction reactions catalysed by aldehyde ferredoxin oxidoreductase (AOR) and alcohol dehydrogenase (ADH) enzymes were incorporated into the metabolic model (the modified MetaCLAU model is detailed in Supplementary File S2). This modified MetaCLAU model was subsequently employed in all the conducted FBAs. To test predictive capability across culture stages, FBA was performed by constraining specific growth, substrate uptake, and ethanol/butanol production rates to experimental data, while maximising acetate production as the objective function, given that is a core WLP product [43], comparing it with the experimentally determined specific uptake of acetate (q_{ACET}).

2.8. Thermodynamic calculations

Changes in Gibbs free energy ($\Delta G'$) for the reduction of acetate to ethanol and butyrate to butanol were calculated to assess the thermodynamic selectivity of solvent production under the experimental conditions. The calculations considered both H_2 and CO as electron donors, according to the reactions shown in Table 2.

The actual Gibbs free energy ($\Delta G'$) at specific time points was calculated according to Eq. (6) [45,46].

$$\Delta G' = \Delta G^0 + RT \ln(Q) \tag{6}$$

Where R is the gas constant (8.314 J mol^{-1} K^{-1}), T is the temperature (310.15 K), and Q is the reaction quotient calculated from the experimental concentrations of liquid metabolites and partial pressures of gases. Henry's law constants (k_H) for H_2, CO, and CO_2 were

Table 2
Standard Gibbs free energy change for acetate and butyrate reduction reactions using CO and H_2 as electron donors at pH 6.0 and 37 °C [44].

Product	Electron donor	Reaction	ΔG^0 [kJ /mol Carboxylate]
Ethanol	CO	$C_2H_3O_2^- + H^+ + 2CO + H_2O \rightarrow C_2H_6O + 2CO_2$	−69.5
	H_2	$C_2H_3O_2^- + H^+ + 2H_2 \rightarrow C_2H_6O + H_2O$	−48.8
Butanol	CO	$C_4H_7O_2^- + H^+ + 2CO + H_2O \rightarrow C_4H_{10}O + 2CO_2$	−77.7
	H_2	$C_4H_7O_2^- + H^+ + 2H_2 \rightarrow C_4H_{10}O + H_2O$	−57.0

Table 3
Specific growth rates of *C. autoethanogenum* in fermentations of gaseous mixtures containing H_2:CO_2 or H_2:CO_2:CO mixtures.

Gas composition	μ [h^{-1}]	Max. biomass conc. [gCDW L^{-1}]	Operational conditions	Reference
90% H_2 + CO_2 mixtures, plus 10% CO	0.052 ± 0.011	0.103 ± 0.008	Batch, headspace pressure 1.5 bar, 150 rpm	This study
90% H_2 + CO_2 mixtures, plus 5% CO	0.028 ± 0.001	0.074 ± 0.009		
90% H_2 + CO_2 mixtures	0.020 ± 0.007	0.062 ± 0.022		
20% H_2, 20% CO_2 & 50% CO	0.040 ± 0.001	0.480 ± 0.040	Chemostat, 50 mL/min gas feeding, 500 rpm	Valgepea et al. [50]
65% H_2, 23% CO_2 & 2% CO	0.042 ± 0.001	0.340 ± 0.020	Chemostat, 30 mL/min gas feeding, 1200 rpm	Heffernan et al. [27]
67% H_2 & 23% CO_2	0.020 ± 0.0004	0.180 ± 0.020	Chemostat, 32 mL/min gas feeding, 500 rpm	
20% H_2, 20% CO_2 & 50% CO	0.116 ± 0.003	1.430 ± 0.030	Chemostat, 72 ml/min gas feeding, 1160 rpm	de Lima et al. [51]
20% H_2, 20% CO_2 & 60% CO	0.065 ± N.D.	0.520 ± N.D.	Batch, 83 mL/min gas feeding, 500 rpm	Oliveira et al. [52]
22% H_2, 9% CO_2 & 30% CO	0.060 ± N.D.	0.540 ± N.D.	Batch, 83 mL/min gas feeding, 1200 rpm	Oppelt et al. [53]
80% H_2 & 20% CO_2	0.025 ± 0.002	0.063 ± N.D.	Batch, headspace pressure 1.75 bar, 100 rpm	Ricci et al. [29]
20% H_2, 20% CO_2 & 50% CO	0.038 ± 0.002	0.273 ± N.D.		

taken from Sander [47] to determine dissolved gas concentrations. The reaction quotients for H_2-driven reduction were defined as:

$$Q_{H2,Acet} = \frac{[\text{Ethanol}]}{[\text{Acetate}^-] \cdot [H_2]^2 \cdot 10^{-pH}} \quad (7)$$

$$Q_{H2,But} = \frac{[\text{Butanol}]}{[\text{Butyrate}^-] \cdot [H_2]^2 \cdot 10^{-pH}} \quad (8)$$

Analogous equations were applied for CO-driven reduction.

3. Results and discussion

The effect of gas composition (H_2:CO_2 ratios and CO supplementation) was assessed on (i) cell growth, substrate consumption and product formation in batch cultures of *C. autoethanoge-num*, and (ii) the solventogenic metabolism of this acetogen, with a focus on ethanol and butanol production.

3.1. Effect of CO supplementation on the growth of C. autoethanogenum during H_2:CO_2 fermentation

Specific growth rates (μ) and maximum biomass concentrations (X_{max}) of *C. autoethanoge-num* were studied during H_2:CO_2 fermentation supplemented with 5% or 10% CO (0.075 and 0.15 bar p_{CO}, respectively). The initial pH was 6.04 ± 0.07, and the final pH remained at 5.59 ± 0.13 across all conditions. This buffering capacity ensured that the culture pH remained within the physiologically active range of pH for this strain (5.5–6.5), preventing significant growth inhibition or product profile changes due to acidification [17,48,49]. Results were compared with previously published data, summarised in Table 3. The average μ obtained in this study using only H_2:CO_2 mixtures (0.020 ± 0.007 h^{-1}) agrees with previously reported values for *C. autoethanogenum* in both chemostat and batch cultures continuously fed by a gaseous mixture containing 80% H_2 and 20% CO_2 [27,29]. This indicates a reproducible baseline for growth performance when H_2 and CO_2 are the sole gaseous carbon and energy sources.

Specific growth rates of *C. autoethanogenum* increased with CO supplementation, indicating that even low p_{CO} can enhance growth. The μ_{max} observed was 0.065 ± 0.003 h^{-1} with a gas mixture of 45% H_2, 45% CO_2, and 10% CO (p_{CO} = 0.15 bar). This μ_{max} is comparable to those reported in batch cultures with continuous syngas supply at higher p_{CO} (0.3–0.6 bar) and higher agitation rates (> 500 rpm) [52,53]. The highest μ_{max} reported to date for *C. autoethanogenum* batch cultures employing H_2, CO_2 and CO mixtures is 0.08 h^{-1}, achieved by Ingelman et al. [54] after adaptive laboratory evolution with a high p_{CO} (0.95 bar) over 107 generations. Thus, the μ_{max} observed in this study approaches the upper range reported for syngas fermentation, although using lower agitation rate and p_{CO}. The average μ with CO supplementation was 0.043 ± 0.015 h^{-1}, comparable to those obtained by Heffernan et al. [27] and Valgepea et al. [50] in chemostat cultures continuously fed with H_2:CO_2 mixtures containing p_{CO} of 0.02 and 0.5 bar, respectively. A comparison of the present study's results with existing literature highlights the significant influence of mass transfer limitations, particularly for CO, on μ values. Ricci et al. [29] observed lower μ in batch cultures using a p_{CO} of 0.88 bar, probably due to a 33% lower agitation rate, which would restrict CO mass transfer into the liquid phase. This critical role of agitation rate in facilitating CO mass transfer and, consequently, improving μ is also evident in continuous systems. For instance, de Lima et al. [51] achieved a higher μ_{max} of 0.116 h^{-1} using the same gas composition as Valgepea et al. [50] (Table 3), but employed a higher gas flow rate and more than double the agitation rate, underscoring the importance of the gaseous mass transfer rate to control *C. autoethanogenum* growth.

A linear regression analysis of average maximum biomass concentrations (X_{max}) obtained across the range of 0 to 0.15 bar of CO supplementation resulted in a biomass yield of 1.52 gCDW $molCO^{-1}$ with a strong correlation (R^2 = 0.948). This experimentally determined yield is in close agreement with the maximum theoretical yield ($Y^{max}_{X/CO}$) of 1.87 gCDW $molCO^{-1}$ reported by Elisiário et al. [55] for continuous cultures using CO as the sole carbon and energy source. This further

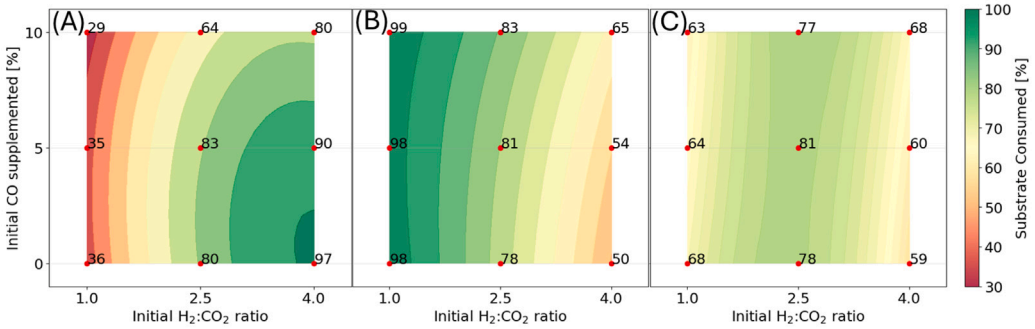

Fig. 2. Consumption of CO_2 (A), H_2 (B) and CO_2 + H_2(C) by *C. autoethanogenum* at 96 h of incubation. Experimental data points are represented by red dots, while the contour plot depicts the response surface equations (Supplementary File S3: Table S1). The corresponding coefficients of determination (R^2) are 0.992, 0.977, and 0.892, respectively.

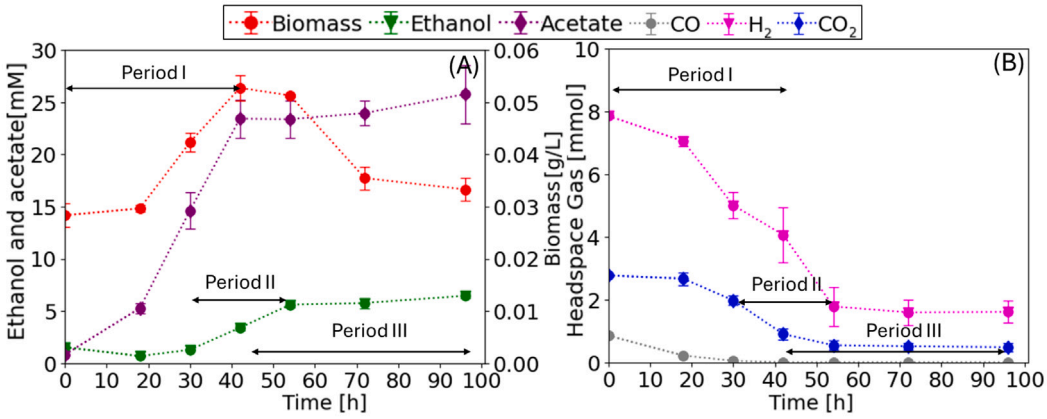

Fig. 3. Example of culture periods defined along the time-dependent concentration profiles of products (A) and substrates (B) at the central point of the factorial design, illustrating period I (exponential growth), period II (solvent production), and period III (post-CO depletion).

supports the efficient incorporation of CO-derived carbon into biomass under the conditions tested.

The observed increase in biomass concentration with increasing CO supplementation can be explained by the preferential utilisation of electrons derived from CO oxidation by CODH for the reduction of ferredoxin. This pivotal step, leads to the regeneration of NADH and NADPH through Ferredoxin:NAD^+-oxidoreductase (Rnf) complex and ferredoxin-dependent transhydrogenase (Nfn), respectively [56]. Consequently, under conditions of low p_{CO}, a substantial portion of the metabolic flux may be directed towards the initial step, i.e.: ATP-independent reduction of CO_2 to formate. This is evidenced by transient extracellular formate accumulation peaking between 17 and 24 h, followed by reassimilation (Supplementary File S3: Figure S1). Notably, the average concentration of accumulated formate was inversely proportional to CO supplementation and shows statistical significance (ANOVA p-value < 0.01), reaching 0.81 mM, 0.63 mM, and 0.29 mM at 0, 0.075, and 0.15 bar p_{CO}, respectively. This diversion of reducing equivalents and carbon towards formate limits the flux through the ATP-generating steps in the WLP leading to acetate production, thereby decreasing overall ATP yield and resulting in reduced biomass production [55]. Conversely, increasing CO concentrations enhances the overall electron donor uptake rate, directly fuelling the generation of reduced ferredoxin and consequently ATP production, enhancing cell growth and biomass accumulation [10]. The observed transient formate excretion and subsequent reassimilation confirms a dynamic metabolic adjustment in response to the changing availability of CO during the first 48 h.

3.2. *Effect of initial CO concentration and H_2:CO_2 molar ratio on H_2 and CO_2 consumption*

Concerning gaseous substrate utilisation, all cultures showed complete consumption of CO within 24–48 h. CO_2 consumption increased with the increase of the initial H_2:CO_2 ratio (Fig. 2A). Addition of CO resulted in a decrease in CO_2 consumption. These results align with preferential CO oxidation, despite the presence of H_2 and CO_2 in the gas headspace, as reported by Xu et al. [57]. At 4:1 H_2:CO_2 molar ratio in absence of CO, 97% of CO_2 was consumed. In contrast, at 2.5:1 H_2:CO_2 molar ratio with 0.15 bar of CO, the total CO_2 consumed was 29%. H_2 consumption decreased from 98% to 50% when the H_2:CO_2 molar ratio increased from 1:1 to 4:1 (Fig. 2B). At 4:1 H_2:CO_2 molar ratio, the increase of CO concentration resulted in an increase in H_2 consumption. This effect is consistent with the increased H_2 demand for CO_2 fixation due to CO-derived CO_2 production. The highest combined consumption occurred at 2.5:1 H_2:CO_2 molar ratio (Fig. 2C). The central point, defined by a 2.5:1 H_2:CO_2 ratio and 0.075 bar of CO, exhibited the maximum combined consumption of 81%. Similarly, optimisation of the second order quadratic equation fitted to the experimental results shows a local maximum of 80% (R^2 = 0.96) combined gas consumption using a 2.4:1 H_2:CO_2 ratio and 0.05 bar of CO. This is consistent with the stoichiometric requirements of 2:1 to 3:1 H_2:CO_2 molar ratios in the WLP for optimal carbon fixation in ethanol and acetate [58,59].

For specific uptake and production rates calculation, time periods were defined for each culture condition (see Supplementary File S1) as shown for the central point of the factorial design in Fig. 3 . During the exponential growth phase (Period I) q_{CO} increased proportionally with initial CO concentration, ranging from 6.8 ± 0.5 to 21.8 ± 8.7 mmol $gCDW^{-1}$ h^{-1} at 0.075 and 0.15 bar p_{CO}, respectively. This direct

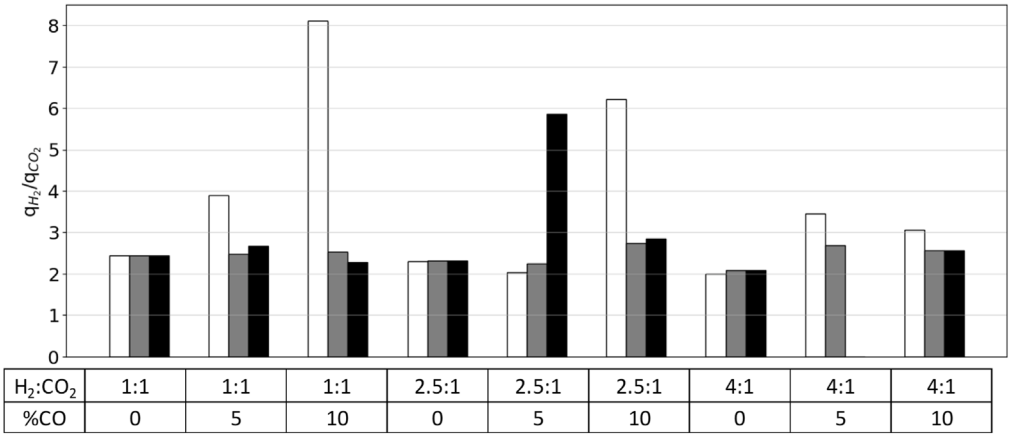

Fig. 4. q_{H_2}/q_{CO_2} ratios during Period I (white bars), Period II (grey bars) and Period III (black bars) for the factorial DoE conditions.

proportionality is in agreement with the findings of Allaart et al. [60]. The average q_{CO} at 0.15 bar p_{CO} closely matches chemostat values (18.8 mmol $gCDW^{-1}$ h^{-1}) obtained using 0.5 bar p_{CO}, 0.2 bar p_{H_2}, and 0.2 bar p_{CO_2} [50]. Once solvent production started (Period II), q_{CO} dropped by ≥50%, even reaching zero due to complete CO consumption during Period I. In contrast, q_{H_2} just decreased from 48.5 ± 12.2 to 37.1 ± 13.0 mmol $gCDW^{-1}$ h^{-1}, with Period I rates similar to chemostat values (47.1 ± 6.7 mol $gCDW^{-1}$ h^{-1}) under 0.8 bar p_{H_2} and 0.2 bar p_{CO_2} [27]. The agreement of specific uptake rates for Period I and previously reported chemostat values suggests that uptake rates can also remain similar during exponential growth, as observed for μ_{max} values.

Despite variability in q_{CO_2}, q_{H_2}/q_{CO_2} ratios ranged from 1.5 to 8.0, increasing with p_{CO} (Fig. 4), reflecting greater H_2 demand to fix CO_2 derived from CO oxidation. In CO-free conditions, the average q_{H_2}/q_{CO_2} ratio was 2.27 ± 0.17, consistent with the 2:1–3:1 H_2:CO_2 ratio stoichiometry required by the WLP for optimal ethanol and acetate formation [58,59]. The observed trends may reflect CO-induced inhibition of hydrogenases [61], limiting CO_2 incorporation from sources other than CO oxidation. Moreover, CO has been reported to influence both uptake rates and μ in acetogenic *Clostridia* [55]. The multiple quadratic polynomial regression of q_{H_2}/q_{CO_2} (Supplementary File S3: Table S2) further confirmed this effect: the coefficients of the quadratic term (C1 vs. C5) and linear term (C4 vs. C7) indicate that CO concentration exerted a stronger influence than H_2:CO_2 ratio, highlighting the strong dependence of uptake fluxes and μ on p_{CO}, particularly at low CO concentrations.

3.3. Effect of H_2:CO_2 ratios and CO supplementation on product formation

Ethanol concentrations increased significantly from 0.7 ± 0.6 mM at 1:1 H_2:CO_2 ratio to 5.5 ± 1.0 mM and 6.0 ± 1.8 mM at H_2:CO_2 ratios of 2.5:1 and 4:1, respectively (ANOVA, p-value < 0.01). This strongly suggests that increasing H_2 partial pressures promotes ethanol production by providing additional reducing power, a phenomenon previously reported by Valgepea et al. [62] in *C. autoethanogenum* chemostat cultures using syngas. In general, ethanol production was also enhanced by increasing p_{CO}, a trend consistent with observations in *C. ljungdahlii* batch cultures grown at H_2:CO ratios varying from 2 to 0.5 [28]. The average acetate concentrations for the experimental conditions shown in Fig. 5 was 24.7 ± 4.7 mM without significant differences (ANOVA, p-value = 0.248). Neither lactate or 2,3-butanediol, as minor by-products of *C. autoethanogenum* CO-driven fermentations [31] were detected.

The highest total product formation (30.7 ± 2.6 mM; acetate plus ethanol) occurred at an H_2:CO_2 ratio of 2.5:1, corresponding to the highest substrate consumption within the defined experimental design range. The carbon yield on C2 products (ethanol and acetate) remained stable across the tested conditions, averaging 91 ± 2%. This suggests that an H_2:CO_2 molar ratio of approximately 2.5:1 may approach the optimal stoichiometric balance for efficient gaseous substrate utilisation while simultaneously promoting a high concentration of C2 products in *C. autoethanogenum* batch cultures under low CO concentrations. The carbon recovery in C2 products obtained here is substantially higher than the 52% value reported by Valgepea et al. [62] in *C. autoethanogenum* chemostat cultures using a syngas mixture containing a p_{CO} of 0.5 bar (20% H_2, 20% CO_2, and 50% CO), where the remaining fraction of the carbon was directed towards CO_2 production. Conversely, our carbon recovery in C2 products is comparable to the 96% reported by Heffernan et al. [27] in *C. autoethanogenum* chemostat cultures employing only H_2:CO_2 mixtures or with minimal 0.02 bar), evidencing the impact of the initial gas composition on carbon distribution.

Specific production rates of acetate (q_{ACET}) halved from 12.2 ± 2.8 to 6.4 ± 2.0 mmol $gCDW^{-1}$ h^{-1} between Period I and II, while specific production rates of ethanol (q_{ETOH}) increased to 1.17 ± 0.87 mmol $gCDW^{-1}$ h^{-1}. Although q_{ETOH} values were more variable, the overall trend indicates that ethanol production started during Period II. The variability was explained by its proportional increase with initial H_2:CO_2 ratios. This is due to the increased availability of H_2 as electron donor. The average q_{ACET} and q_{ETOH} values observed during Period II are consistent with those reported in chemostat cultures (6.4 and 1.2 mmol $gCDW^{-1}$ h^{-1}, respectively) using syngas containing 0.5 bar p_{CO}, 0.2 bar p_{H_2}, and 0.2 bar p_{CO_2} [50]. Notably, changing the primary electron donor from CO to H_2 promotes a higher proportion of q_{ETOH} relative to q_{ACET}. Although ethanol production from CO is energetically superior [63], under H_2-dependent conditions (Period III) acetate and ethanol synthesis become energetically equivalent (~0.3 ATP/product via AOR pathway). In this state, metabolism is driven by the need to balance the reducing equivalents generated by H_2 oxidation. Since ethanol formation serves as an electron sink, consuming 4 electrons per acetyl-CoA compared to none for acetate, flux is directed towards solvent production to maintain redox homeostasis. Consequently, the q_{ETOH}/q_{ACET} ratio increased throughout cultivation, particularly during Period III, as shown in Fig. 6. This trend was most pronounced at the central point condition (2.5:1 H_2:CO_2, 0.075 bar p_{CO}), where ethanol production finished around 55 h (approx. 35 h after the onset of Period II). This prolonged solventogenic activity required a higher stoichiometric input of electrons compared to acetate formation (3H_2 per CO_2 vs 2H_2 per CO_2, respectively [58,59]), providing a metabolic explanation for the distinct increase in the specific H_2 uptake ratio (q_{H_2}/q_{CO_2}) observed for this condition in Fig. 4.

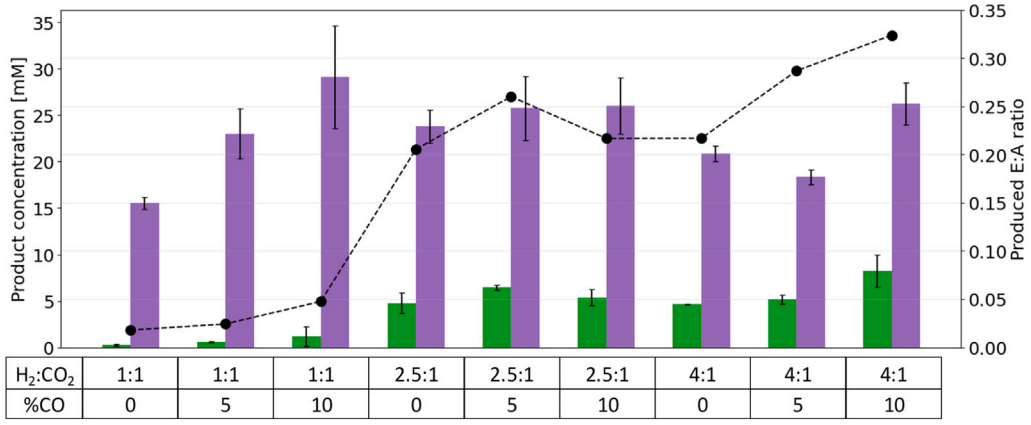

H_2:CO_2	1:1	1:1	1:1	2.5:1	2.5:1	2.5:1	4:1	4:1	4:1
%CO	0	5	10	0	5	10	0	5	10

Fig. 5. Concentrations of ethanol (green bars), acetate (purple bars) and E:A molar ratios (black dots) measured at 96 h for the factorial DoE conditions. At the bottom of the figure initial H_2:CO_2 ratio and CO supplementation are indicated.

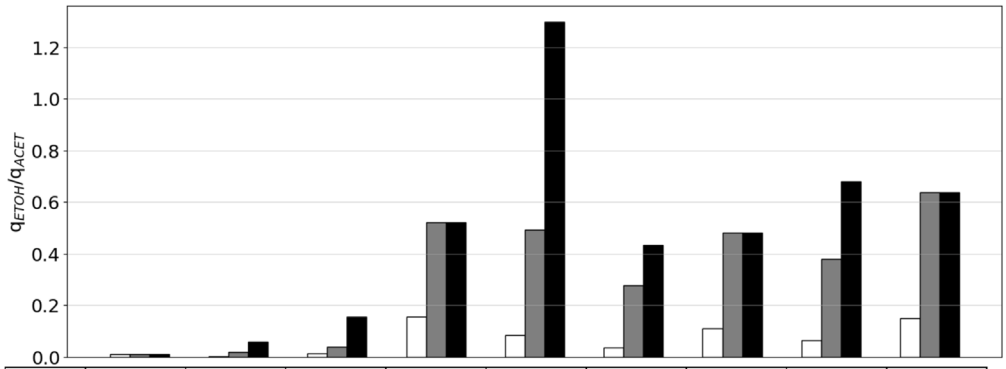

H_2:CO_2	1:1	1:1	1:1	2.5:1	2.5:1	2.5:1	4:1	4:1	4:1
%CO	0	5	10	0	5	10	0	5	10

Fig. 6. q_{ETOH}/q_{ACET} ratios during Period I (white bars), Period II (grey bars) and Period III (black bars), for the factorial DoE conditions.

3.4. Reduction of butyrate to butanol by C. autoethanogenum under variable H_2:CO_2:CO head-space

The central point of the factorial design, characterised by the highest consumption of H_2 and CO_2 with one of the highest product concentrations and E:A ratios, was selected as the basis for the subsequent Box–Behnken design to investigate the impact of butyrate addition on *C. autoethanogenum* metabolism. Although increasing butyrate concentrations resulted in a statistically higher initial pH (ANOVA *p*-value < 0.01), the variation was biologically negligible (6.00 ± 0.08 to 6.08 ± 0.06, CV = 1.15%), and no significant differences were observed in the final pH (ANOVA *p*-value = 0.77). This confirms that the buffering capacity effectively maintained physiological conditions across all butyrate concentrations, indicating that the marginal differences in initial pH did not significantly altered the culture. All incubations, both without CO and with low CO (10%) in the headspace, showed butyrate reduction to butanol (Fig. 7). At the two butyrate concentrations tested, an H_2:CO_2 ratio of 1:1 (lowest H_2 percentage tested) resulted in the lowest butyrate-to-butanol conversion (9.3 ± 2.8%), likely attributed to insufficient H_2 for the required reduction steps. Increasing the H_2:CO_2 ratio to 2.5:1 - 4:1 resulted in a 2 to 3 times higher butanol concentration, highlighting the correlation between H_2 availability and carboxylate reduction metabolism [62]. CO supplementation exhibited a lower impact than increasing H_2:CO_2 ratios on the final butanol concentration, with increases reaching up to 1.5 times the concentration observed in its absence. However, CO promoted the onset of butyrate reduction, with conversion starting on the first day of culture, in contrast to the lag of 48 h observed under CO-free conditions. This early onset suggests that inducing solvent production prior to the stationary phase may be a pivotal step for targeted solvent production. For example, Diender et al. [19] reported no butanol formation when adding 8 mM butyrate to a *C. autoethanogenum* chemostat on day six, after stationary phase was reached, under a CO:H_2 ratio of 2:1. Thus, timely initiating the production of solvents emerges as a critical factor in enhancing butanol yields from butyrate. In CO supplemented cultures, specific production rates of butanol (q_{BUTOH}) reached 0.95 ± 0.29 and 1.53 ± 0.37 mmol $gCDW^{-1}$ h^{-1} at 0.075 and 0.15 bar pCO, respectively, during Period I. However, these rates declined by 59 ± 21% during Period II, likely due to CO depletion and diversion of reducing equivalents to reduce acetate to ethanol. In contrast, cultures grown solely on H_2 and CO_2 exhibited delayed butyrate reduction, with q_{BUTOH} of 1.15 ± 0.68 mmol $gCDW^{-1}$ h^{-1}.

These findings highlight the trade-off between CO and H_2 in *C. autoethanogenum* carboxylate reduction pathways. While CO enhances growth and provides the necessary reduced ferredoxin and NADH for earlier butyrate reduction, H_2 plays a crucial role in CO_2 fixation and subsequent reduction of carboxylates (i.e. acetate and butyrate). Enhanced H_2 availability stimulates NADPH generation via the hydrogenase complex (HYT). Excess NADPH is recycled to NADP+ through the Nfn enzyme, simultaneously producing reduced ferredoxin and NADH. Carboxylate reduction through AOR and ADH enzymes acts as an electron sink, maintaining cellular redox balance and energy homeostasis. Thus, the regeneration of ferredoxin and NADH requires fewer enzymatic steps than through the WLP. Despite the positive influence of H_2 on carboxylate reduction, total H_2 consumption varied by less than 10% relative to butyrate-free controls. This is consistent with

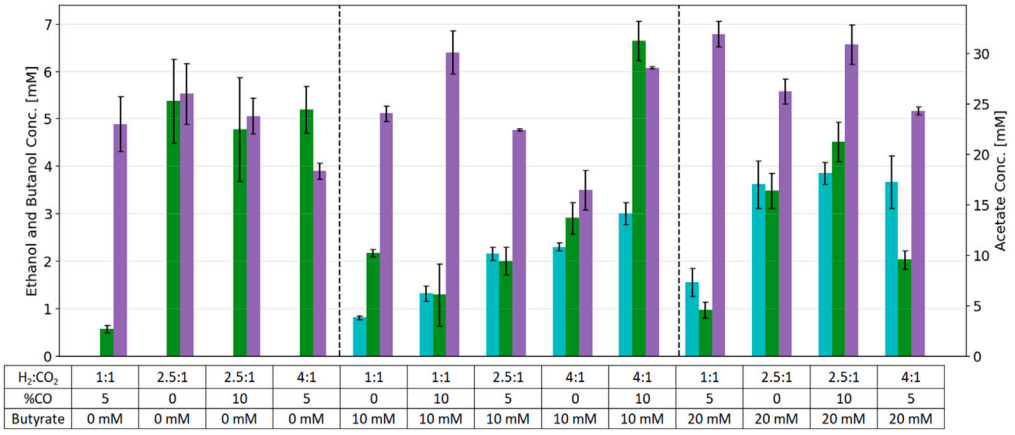

H_2:CO_2	1:1	2.5:1	2.5:1	4:1	1:1	1:1	2.5:1	4:1	4:1	1:1	2.5:1	2.5:1	4:1
%CO	5	0	10	5	0	10	5	0	10	5	0	10	5
Butyrate	0 mM	0 mM	0 mM	0 mM	10 mM	10 mM	10 mM	10 mM	10 mM	20 mM	20 mM	20 mM	20 mM

Fig. 7. Butanol (turquoise), ethanol (green) and acetate (purple) concentrations measured in *C. autoethanogenum* cultures at 96 h grouped by initial butyrate concentration, for the Box–Behnken DoE conditions. At the bottom of the figure initial H_2:CO_2 ratio, CO supplementation and butyrate concentrations are indicated.

prior observations in *C. ljungdahlii*, where a relatively low proportion of the electrons derived from CO and H_2 oxidation was allocated to butyrate reduction, resulting in approximately a 6% increase in H_2 consumption [24].

Fig. 7 shows that higher addition of butyrate increased the butanol concentrations produced. However, it should be noted that this increase in butyrate concentration resulted in lower substrate conversion rates. Specifically, the maximum butanol concentrations reached with 10 mM and 20 mM butyrate additions were 3.0 ± 0.2 mM and 3.6 ± 0.1 mM, respectively. A comparison of the moles of butanol produced to the moles of butyrate consumed for each condition revealed discrepancies of 6.7 ± 4.2% (<1 mM). This differences could be attributed to the inherent limitations of the analytical method at low concentrations (≤ 10 mM). To date, no alternative pathway or enzyme has been identified in *C. autoethanogenum* or closely related strains that could incorporate butyrate or butanol into other metabolic routes beyond the reduction/oxidation reactions catalysed by aldehyde ferredoxin oxidoreductase (AOR) and alcohol dehydrogenase (ADH) [8,11,24].

The H_2:CO_2 ratio significantly influences alcohol production in *C. autoethanogenum* batch cultures, mainly due to the availability of H_2 as an electron donor for acetate reduction to ethanol. While the reduction of carboxylic acids to alcohols driven solely by molecular hydrogen has been demonstrated in biocatalytic systems using the hyperthermophile *Pyrococcus furiosus* [64], studies on carboxylate reduction in acetogens have predominantly utilised fixed syngas compositions characterised by high partial pressures of CO [8,24]. The reduction of butyrate to butanol is intrinsically linked to CO_2 fixation, as evidenced by the formation of a complex between the bifurcating hydrogenase (HYT) and formate dehydrogenase (FDH) enzymes [56]. The activity of this complex drastically decreases when CO_2 availability becomes limiting, potentially restricting hydrogen utilisation and further carboxylates reduction. Consequently, both H_2 and CO_2 could act as limiting substrates in butyrate reduction.

The tested CO supplementation (0%–10%) suggests an interesting solvent production potential at higher percentages. Increased CO could enhance electron availability, potentially boosting ethanol and butanol concentrations produced, but may also increase byproducts formation like CO_2 or butanediol, compromising selectivity for acetate and ethanol [29,31] and shifting the process away from CO_2 utilisation as feedstock. For instance, Moreira et al. [33] reported that in *C. autoethanogenum* batch cultures (H_2:CO_2 = 4:1, 0.8 bar headspace), increasing p_{CO} from 0.19 to 0.36 bar decreased CO_2 utilisation from 82% to 73%. At higher supplementation (up to 1.1 bar, 60% CO), the carbon yield of acetate dropped from 96% to 67%, mainly due to initial CO_2 production. These findings suggest that while higher CO levels may enhance reduction capacity, they also introduce trade-offs in selectivity and carbon efficiency. Future work should expand CO supplementation studies to better define these trade-offs and optimise electron donor use for target product formation.

Butyrate addition did not significantly influence acetate production by *C. autoethanogenum* (ANOVA, *p*-value = 0.17), with an average acetate concentration of 24.6 ± 5.0 mM measured at the end of incubations (Fig. 7). This final acetate concentration is similar to butyrate-free cultures (Fig. 5). Conversely, ethanol production exhibited a substantial decrease in the presence of butyrate, ranging from a 20% to 70% reduction, which affects the E:A molar ratio produced. Consequently, the maximum E:A ratio was 0.29 in butyrate-free cultures, decreasing to 0.23 and 0.14 with the addition of 10 mM and 20 mM initial butyrate, respectively (Fig. 8). The observed decrease in ethanol formation is attributed to competition for reducing equivalents, specifically ferredoxin and NADH, between acetate and butyrate reduction pathways. The presence of butyrate from the start of fermentation likely leads to a preferential utilisation of these redox cofactors towards butyrate-to-butanol reduction, a process requiring fewer enzymatic steps than acetate reduction to ethanol.

3.5. Modelling the effect of gas composition and butyrate addition in C. autoethanogenum metabolism

To obtain mechanistic insights into the impact of varying gas compositions on product distribution in the batch cultures, internal flux distribution was estimated through FBA. For model selection, the ethanol-to-acetate (E:A) flux ratio was selected as the parameter that represent the distribution between the targeted products, comparing it with the experimentally determined E:A ratio of 2.71 reported by Heffernan et al. [27] for a *C. autoethanogenum* continuous culture grown on a gas mixture with 67% H_2, 23% CO_2, and 2% CO. Among the evaluated Genome-scale models (GEMs MetaCLAU [31], iCLAU786 [40], and iHN637 [41]), the MetaCLAU model exhibited the closest predictive capability, with an E:A flux ratio of 2.73. In contrast, the iCLAU786 and iHN637 models predicted significantly different E:A flux ratios of 9.91 and 3.31, respectively. Based on this comparative analysis, the MetaCLAU model was chosen as the most suitable foundation for our FBA. The obtained q_{ACET} averaged 11.1 ± 6.2 and 4.3 ± 2.3 mmol $gCDW^{-1}$ h^{-1} during Periods I and II, respectively (Fig. 9). Model predictions matched experimental values with 95 ± 28% agreement, and 15 of 18 conditions showed <30% deviation (R^2 = 0.89).

The FBA-based flux indicated that ATP generation decreased more sharply than fluxes of NADH, NADPH and Fd_{red} produced over time, particularly when CO was depleted at 20–25 h. Consequently, the q_{NADH}/q_{ATP} ratio increased from 1.2 ± 0.3 in Period I to 1.4 ± 0.2 during Period II, reaching 1.7 ± 0.2 in Period III (Fig. 10). These changes

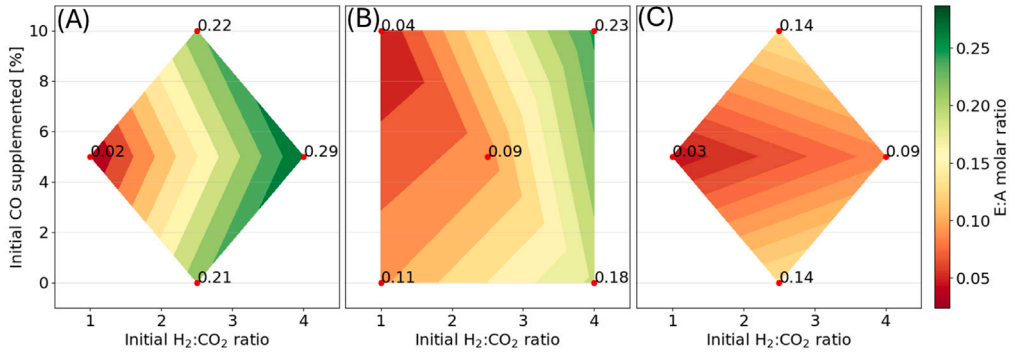

Fig. 8. *C. autoethanogenum* E:A molar ratio produced, grouped by initial butyrate added: (A) 0 mM, (B) 10 mM and (C) 20 mM for the Box–Behnken DoE conditions. The contour plot depicts the response surface equation for E:A ratio (Supplementary File S3: Table S2), with a corresponding R^2 of 0.991.

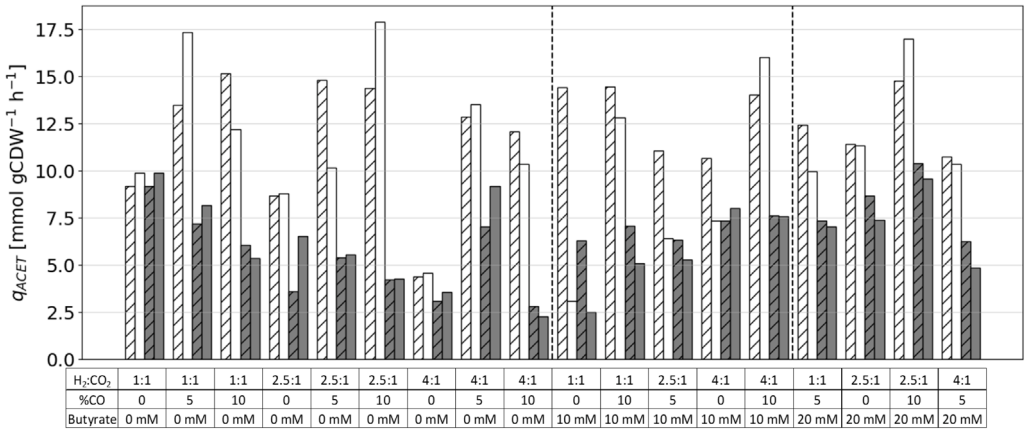

Fig. 9. Comparison between experimental data (patterned bars) and FBA predictions (solid bars) for specific acetate production rates during Period I (white bars) and Period II (grey bars) for all the experimental conditions.

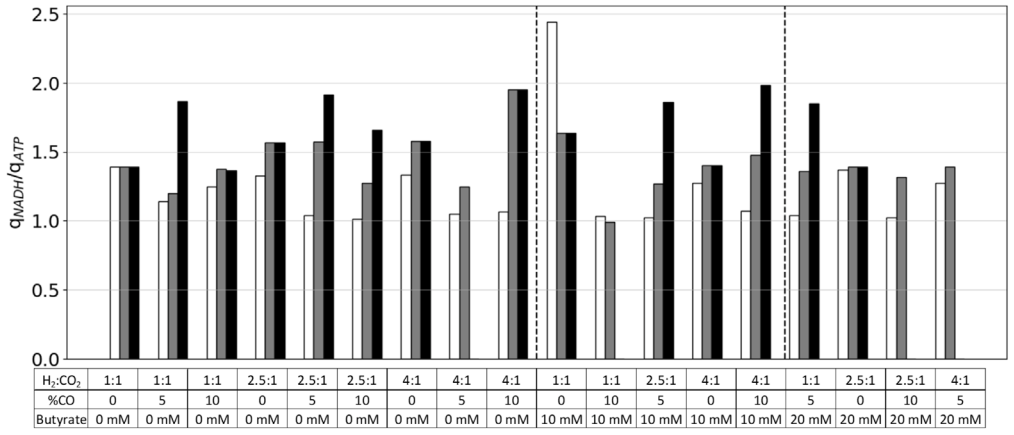

Fig. 10. FBA determined q_{NADH}/q_{ATP} ratios during Period I(white bars), Period II (grey bars) and Period III (black bars) for all the experimental conditions.

in q_{NADH}/q_{ATP} ratios coincided with the onset of ethanol production, occurring at 25 h in cultures without butyrate and at 50 h when butyrate was added. Similar trends were observed for q_{NADPH}/q_{ATP} (+42%) and $q_{Fd_{red}}/q_{ATP}$ (+29%). These results suggest that Period II is driven by the relative availability of reducing equivalents compared to the availability of ATP.

The proportion of NADH consumed by the ADH enzyme to reduce butyraldehyde to butanol averaged 4.7 ± 1.6% of the total NADH flux during both Periods I and II. In contrast, the use of NADH for the reduction of acetaldehyde to ethanol showed greater variability. In cultures supplemented with butyrate, this flux increased from 1.9 ± 2.5 during Period I to 5.8 ± 3.2% during Period II. Without butyrate, the corresponding increase was from 3.0 ± 2.6 to 7.2 ± 6.5%. Similar patterns were observed for Fd_{red} utilisation by AOR in butyrate and acetate reduction to their respective aldehydes, with proportions ranging from 1 to 5%. These values are consistent with the low variations

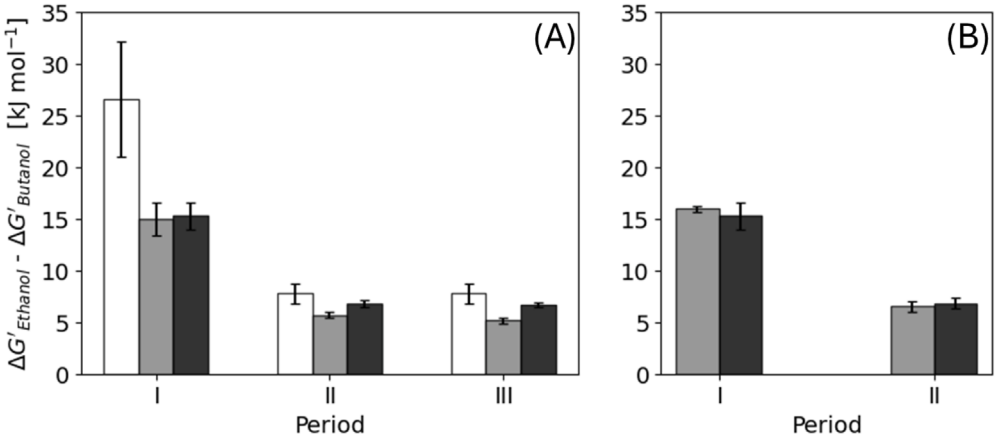

Fig. 11. Average differential Gibbs free energy change ($\Delta\Delta G' = \Delta G'_{Ethanol} - \Delta G'_{Butanol}$) for the defined fermentation periods, with p_{CO} of 0 bar (white bars), 0.075 bar (grey bars), and 0.15 bar (black bars) for both H_2 (A) and CO (B).

in H_2 consumption (<10%) observed upon butyrate addition. These results support the idea that a minor fraction of the electron flux is directed to solvent production pathways, even in the presence of external carboxylates [24]. The presence of butyrate at the start of the fermentation, likely imposed an early redirection of redox cofactors to butyrate reduction, thereby constraining the electron flux available for the acetate-to-ethanol reductive pathway. Furthermore, experimental data shows that in the presence of butyrate, ethanol production begins when acetate concentrations exceed butyrate concentrations, around 50 h (Supplementary File S1). The reduced number of enzymatic steps required for butyrate reduction, compared to the production of acetyl-CoA via the WLP followed by the reduction of acetate to ethanol, contributes to the lower concentrations of ethanol reached in butyrate-supplemented cultures. FBA also revealed that hydrogenase (Hyt) activity was present during CO consumption, suggesting that part of the CO_2 was reduced to formate using H_2 through the formate-H_2 lyase activity of the HytA-E/FdhA enzyme complex [56]. This electron-bifurcating pathway ensures CO_2 reduction in the WLP, allowing H_2 coutilisation. This effect represents a potential advantage of increasing H_2 concentrations compared to using CO as the sole energy source [50].

The metabolic model captured key aspects of *C. autoethanogenum* metabolism but its predictive capacity was limited by assumptions of balanced growth, uptake, and production rates, which does not fully reflect the dynamic nature of metabolic processes. This study combines factorial and Box–Behnken designs with metabolic modelling to provide a framework linking gas composition to solvent production pathways, highlighting redox and energy interplay. Future work will develop a dynamic FBA (dFBA) approach integrating substrate uptake kinetics and multi-substrate consumption models, alongside process parameter optimisation, to enhance predictions of metabolic fluxes, product distributions, concentration profiles, and selectivity in batch gas fermentation systems.

3.6. Thermodynamic prioritisation of solvent production

The prioritisation of butanol over ethanol production can be thermodynamically explained. As calculated by Isom et al. [8], the reduction of butyrate to butanol is energetically more favourable than the reduction of acetate to ethanol. When CO serves as the electron donor, the standard Gibbs free energy change ($\Delta G^{0'}$) for butyrate reduction is approximately 40% more negative than for acetate reduction (Table 2). Even when H_2 is the reductant, butyrate reduction $\Delta G^{0'}$ exceeds by 17% the one needed for the reduction of acetate [8]. This gradient can create a strong driving force that directs reducing equivalents towards the AOR/ADH pathway for butyrate conversion, outcompeting the thermodynamically steeper energy requirements to initiate ethanol production.

To determine how this theoretical advantage affects our specific experimental conditions, we analysed the evolution of the Gibbs free energy change ($\Delta G'$) throughout the fermentation. Fig. 11 illustrates the average differential driving force ($\Delta\Delta G' = \Delta G'_{Ethanol} - \Delta G'_{Butanol}$). A positive $\Delta\Delta G'$ value indicates that the reduction of butyrate to butanol is thermodynamically more favourable than the reduction of acetate to ethanol. Consistent with the theoretical standard potentials, the actual $\Delta G'$ disparity at the onset of fermentation is substantial ($\Delta\Delta G' > 32$ kJ/mol). This gap is driven by specific experimental conditions: the presence of exogenous butyrate (10–20 mM) creates a highly favourable quotient ($Q_{But} \ll Q_{Acet}$). However, as fermentation progresses ($t > 30$ h), this gap narrows to approximately 5–7 kJ/mol due to the accumulation of acetate (increasing the driving force for ethanol production) and butanol (decreasing the driving force for butyrate reduction). This can explain the experimentally observed product profiles: the system initially favours butyrate reduction, but as $\Delta G'$ difference narrows around 30 h, the metabolic flux is increasingly partitioned towards ethanol production to satisfy redox homeostasis. During period I, CO supplementation resulted in a significant decrease of $\Delta\Delta G'$ (T-test, p-value < 0.01), due to the earlier onset of butyrate reduction to butanol and the increased growth rates associated with higher acetate production fluxes, boosting the described narrowing effect between $\Delta G'_{Ethanol}$ and $\Delta G'_{Butanol}$.

4. Conclusion

This study highlights the metabolic versatility of *C. autoethanogenum* in syngas fermentation, particularly its ability to reduce butyrate to butanol using either H_2 or CO as electron donors. Increasing H_2:CO_2 ratios enhanced CO_2 utilisation and stimulated alcohol production pathways, favouring the reduction of externally supplied butyrate over endogenously produced acetate. CO supplementation enhanced growth and promoted earlier butyrate reduction due to preferential CO oxidation, whereas low CO partial pressures in butyrate-free cultures enabled the production of ethanol and acetate with high selectivity and negligible byproducts. Moreover, H_2 incorporation depends on CO_2 availability, while CO oxidation generates additional CO_2, reducing carbon fixation efficiency and highlighting a trade-off between H_2 and CO, with favourable outcomes observed at a 2.5:1 H_2:CO_2 ratio. The delayed onset of ethanol formation during butyrate-to-butanol conversion suggests competition for NADH and Fd_{red}.

CRediT authorship contribution statement

Andrés Suazo: Writing – original draft, Visualization, Validation, Software, Methodology, Investigation, Funding acquisition, Formal analysis, Data curation, Conceptualization. **Ivette Parera Olm:** Writing – review & editing, Validation, Supervision, Methodology, Investigation. **Fabián Otálora:** Writing – review & editing, Data curation. **Jimmy Martínez-Ruano:** Writing – review & editing, Resources. **Raúl Conejeros:** Writing – review & editing, Supervision, Methodology, Funding acquisition, Conceptualization. **Germán Aroca:** Writing – review & editing, Supervision, Methodology, Funding acquisition, Conceptualization. **Diana Z. Sousa:** Writing – review & editing, Supervision, Resources, Methodology, Funding acquisition, Conceptualization.

Declaration of competing interest

The authors declare that they have no known competing financial interests or personal relationships that could have appeared to influence the work reported in this paper.

Acknowledgment

This study was financially supported by the Dutch Research Council (NWO) through the MicroSynC project (Perspective Program P16-10/1) and by the National Agency for Research and Development (ANID-Chile) through the project ANILLO ATE 220045 and the Ph.D. scholarship of Andrés Suazo (ANID National Doctoral Scholarship grant 21201429).

Appendix A. Supplementary data

Supplementary material related to this article can be found online at https://doi.org/10.1016/j.cej.2026.172982.

Data availability

Data will be made available on request.

References

[1] M. Köpke, S.D. Simpson, Pollution to products: recycling of 'above ground'carbon by gas fermentation, Curr. Opin. Biotechnol. 65 (2020) 180–189, http://dx.doi.org/10.1016/j.copbio.2020.02.017.

[2] E. Ahmad, S. Upadhyayula, K.K. Pant, et al., Biomass-derived CO2 rich syngas conversion to higher hydrocarbon via Fischer-Tropsch process over Fe–Co bimetallic catalyst, Int. J. Hydrog. Energy 44 (51) (2019) 27741–27748, http://dx.doi.org/10.1016/j.ijhydene.2019.09.015.

[3] S. Wan, M. Lai, X. Gao, M. Zhou, S. Yang, Q. Li, F. Li, L. Xia, Y. Tan, Recent progress in engineering Clostridium autoethanogenum to synthesize the biochemicals and biocommodities, Synth. Syst. Biotechnol. 9 (1) (2024) 19–25, http://dx.doi.org/10.1016/j.synbio.2023.12.001.

[4] N. Fackler, B.D. Heijstra, B.J. Rasor, H. Brown, J. Martin, Z. Ni, K.M. Shebek, R.R. Rosin, S.D. Simpson, K.E. Tyo, R.J. Giannone, R.L. Hettich, T.J. Tschaplinski, C. Leang, S.D. Brown, M.C. Jewett, M. Köpke, Stepping on the gas to a circular economy: accelerating development of carbon-negative chemical production from gas fermentation, Annu. Rev. Chem. Biomol. Eng. 12 (2021) 439–470, http://dx.doi.org/10.1146/annurev-chembioeng-120120-021122.

[5] R.M. Handler, D.R. Shonnard, E.M. Griffing, A. Lai, I. Palou-Rivera, Life cycle assessments of ethanol production via gas fermentation: anticipated greenhouse gas emissions for cellulosic and waste gas feedstocks, Ind. Eng. Chem. Res. 55 (12) (2016) 3253–3261, http://dx.doi.org/10.1021/acs.iecr.5b03215.

[6] A. Poehlein, B. Zeldes, M. Flaiz, T. Böer, A. Lüschen, F. Höfele, K.S. Baur, B. Molitor, C. Kröly, M. Wang, Q. Zhang, Y. Fan, W. Chao, R. Daniel, F. Li, M. Basen, V. Müller, L.T. Angenent, D.Z. Sousa, F.R. Bengelsdorf, Advanced aspects of acetogens, Bioresour. Technol. 427 (2025) 131913, http://dx.doi.org/10.1016/j.biortech.2024.131913.

[7] J. Mock, Y. Zheng, A.P. Mueller, S. Ly, L. Tran, S. Segovia, S. Nagaraju, M. Köpke, P. Dürre, R.K. Thauer, Energy conservation associated with ethanol formation from H2 and CO2 in clostridium autoethanogenum involving electron bifurcation, J. Bacteriol. 197 (18) (2015) 2965–2980, http://dx.doi.org/10.1128/jb.00399-15.

[8] C.E. Isom, M.A. Nanny, R.S. Tanner, Improved conversion efficiencies for n-fatty acid reduction to primary alcohols by the solventogenic acetogen "*Clostridium ragsdalei*", J. Ind. Microbiol. Biotechnol. 42 (1) (2015) 29–38, http://dx.doi.org/10.1007/s10295-014-1543-z.

[9] H. Richter, B. Molitor, M. Diender, D.Z. Sousa, L.T. Angenent, A narrow pH range supports butanol, hexanol, and octanol production from syngas in a continuous co-culture of *Clostridium ljungdahlii* and *Clostridium kluyveri* with in-line product extraction, Front. Microbiol. 7 (2016) 215073, http://dx.doi.org/10.3389/fmicb.2016.01773.

[10] M.T. Allaart, M. Diender, D.Z. Sousa, R. Kleerebezem, Overflow metabolism at the thermodynamic limit of life: How carboxydotrophic acetogens mitigate carbon monoxide toxicity, Microb. Biotechnol. 16 (4) (2023) 697–705, http://dx.doi.org/10.1111/1751-7915.14212.

[11] M. Diender, J.C. Dykstra, I. Parera Olm, S.W. Kengen, A.J. Stams, D.Z. Sousa, The role of ethanol oxidation during carboxydotrophic growth of *Clostridium autoethanogenum*, Microb. Biotechnol. 16 (11) (2023) 2082–2093, http://dx.doi.org/10.1111/1751-7915.14338.

[12] J. Bae, C. Park, H. Jung, S. Jin, B.-K. Cho, Harnessing acetogenic bacteria for one-carbon valorization toward sustainable chemical production, RSC Chem. Biol. 5 (9) (2024) 812–832, http://dx.doi.org/10.1039/D4CB00099D.

[13] L. Jourdin, M. Winkelhorst, B. Rawls, C.J. Buisman, D.P. Strik, Enhanced selectivity to butyrate and caproate above acetate in continuous bioelectrochemical chain elongation from CO_2: steering with CO_2 loading rate and hydraulic retention time, Bioresour. Technol. Rep. 7 (2019) 100284, http://dx.doi.org/10.1016/j.biteb.2019.100284.

[14] Á. Fernández-Naveira, M.C. Veiga, C. Kennes, Selective anaerobic fermentation of syngas into either C2-C6 organic acids or ethanol and higher alcohols, Bioresour. Technol. 280 (2019) 387–395, http://dx.doi.org/10.1016/j.biortech.2019.02.018.

[15] J.R. Phillips, H.K. Atiyeh, R.S. Tanner, J.R. Torres, J. Saxena, M.R. Wilkins, R.L. Huhnke, Butanol and hexanol production in *Clostridium carboxidivorans* syngas fermentation: medium development and culture techniques, Bioresour. Technol. 190 (2015) 114–121, http://dx.doi.org/10.1016/j.biortech.2015.04.043.

[16] C. Fernández-Blanco, M.C. Veiga, C. Kennes, Efficient production of n-caproate from syngas by a co-culture of *Clostridium aceticum* and *Clostridium kluyveri*, J. Environ. Manag. 302 (2022) 113992, http://dx.doi.org/10.1016/j.jenvman.2021.113992.

[17] M. Diender, A.J. Stams, D.Z. Sousa, Production of medium-chain fatty acids and higher alcohols by a synthetic co-culture grown on carbon monoxide or syngas, Biotechnol. Biofuels 9 (2016) 1–11, http://dx.doi.org/10.1186/s13068-016-0495-0.

[18] T. Haas, R. Krause, R. Weber, M. Demler, G. Schmid, Technical photosynthesis involving CO_2 electrolysis and fermentation, Nat. Catal. 1 (1) (2018) 32–39, http://dx.doi.org/10.1038/s41929-017-0005-1.

[19] M. Diender, I. Parera Olm, M. Gelderloos, J.J. Koehorst, P.J. Schaap, A.J. Stams, D.Z. Sousa, Metabolic shift induced by synthetic co-cultivation promotes high yield of chain elongated acids from syngas, Sci. Rep. 9 (1) (2019) 18081, http://dx.doi.org/10.1038/s41598-019-54445-y.

[20] I.P.W. Dharmasiddhi, J. Chen, B. Arab, C. Lan, C. Euler, C.P. Chou, Y. Liu, Engineering a cross-feeding synthetic bacterial consortium for degrading mixed PET and Nylon monomers, Processes 13 (2) (2025) 375, http://dx.doi.org/10.3390/pr13020375.

[21] H. Seo, G. Castro, C.T. Trinh, Engineering a synthetic *Escherichia coli* coculture for compartmentalized *de novo* biosynthesis of isobutyl butyrate from mixed sugars, ACS Synth. Biol. 13 (1) (2023) 259–268, http://dx.doi.org/10.1021/acssynbio.3c00493.

[22] J.C. Liao, L. Mi, S. Pontrelli, S. Luo, Fuelling the future: microbial engineering for the production of sustainable biofuels, Nat. Rev. Microbiol. 14 (5) (2016) 288–304, http://dx.doi.org/10.1038/nrmicro.2016.32.

[23] S. Benito-Vaquerizo, M. Diender, I.P. Olm, V.A.M. Dos Santos, P.J. Schaap, D.Z. Sousa, M. Suarez-Diez, Modeling a co-culture of *Clostridium autoethanogenum* and *Clostridium kluyveri* to increase syngas conversion to medium-chain fatty-acids, Comput. Struct. Biotechnol. J. 18 (2020) 3255–3266, http://dx.doi.org/10.1016/j.csbj.2020.10.003.

[24] J.M. Perez, H. Richter, S.E. Loftus, L.T. Angenent, Biocatalytic reduction of short-chain carboxylic acids into their corresponding alcohols with syngas fermentation, Biotechnol. Bioeng. 110 (4) (2013) 1066–1077, http://dx.doi.org/10.1002/bit.24786.

[25] Y. Liu, F. Lü, L. Shao, P. He, Alcohol-to-acid ratio and substrate concentration affect product structure in chain elongation reactions initiated by unacclimatized inoculum, Bioresour. Technol. 218 (2016) 1140–1150, http://dx.doi.org/10.1016/j.biortech.2016.07.067.

[26] Y. Yin, Y. Zhang, D.B. Karakashev, J. Wang, I. Angelidaki, Biological caproate production by *Clostridium kluyveri* from ethanol and acetate as carbon sources, Bioresour. Technol. 241 (2017) 638–644, http://dx.doi.org/10.1016/j.biortech.2017.05.184.

[27] J.K. Heffernan, K. Valgepea, R. de Souza Pinto Lemgruber, I. Casini, M. Plan, R. Tappel, S.D. Simpson, M. Köpke, L.K. Nielsen, E. Marcellin, Enhancing CO_2-valorization using *Clostridium autoethanogenum* for sustainable fuel and chemicals production, Front. Bioeng. Biotechnol. 8 (2020) 204, http://dx.doi.org/10.3389/fbioe.2020.00204.

[28] J. Jack, J. Lo, P.-C. Maness, Z.J. Ren, Directing *Clostridium ljungdahlii* fermentation products via hydrogen to carbon monoxide ratio in syngas, Biomass Bioenergy 124 (2019) 95–101, http://dx.doi.org/10.1016/j.biombioe.2019.03.011.

[29] L. Ricci, V. Agostino, D. Fino, A. Re, Screening of gas substrate and medium effects on 2, 3-Butanediol production with *C. ljungdahlii* and *C. autoethanogenum* aided by improved autotrophic cultivation technique, Fermentation 7 (4) (2021) 264, http://dx.doi.org/10.3390/fermentation7040264.

[30] I. Parera Olm, D.Z. Sousa, Upgrading dilute ethanol to odd-chain carboxylic acids by a synthetic co-culture of *Anaerotignum neopropionicum* and *Clostridium kluyveri*, Biotechnol. Biofuels Bioprod. 16 (1) (2023) 83, http://dx.doi.org/10.1186/s13068-023-02336-w.

[31] R.O. Norman, T. Millat, S. Schatschneider, A.M. Henstra, R. Breitkopf, B. Pander, F.J. Annan, P. Piatek, H.B. Hartman, M.G. Poolman, D.A. Fell, K. Winzer, N.P. Minton, C. Hodgman, Genome-scale model of *C. autoethanogenum* reveals optimal bioprocess conditions for high-value chemical production from carbon monoxide, Eng. Biol. 3 (2) (2019) 32–40, http://dx.doi.org/10.1049/enb.2018.5003.

[32] M. Bäumler, M. Schneider, A. Ehrenreich, W. Liebl, D. Weuster-Botz, Synthetic co-culture of autotrophic *Clostridium carboxidivorans* and chain elongating *Clostridium kluyveri* monitored by flow cytometry, Microb. Biotechnol. 15 (5) (2022) 1471–1485, http://dx.doi.org/10.1111/1751-7915.13941.

[33] J.P. Moreira, L. Domingues, J.I. Alves, Metabolic versatility of acetogens in syngas fermentation: Responding to varying CO availability, Bioresour. Technol. 417 (2025) 131823, http://dx.doi.org/10.1016/j.biortech.2024.131823.

[34] C. Yuangyai, H. Nembhard, Chapter 8 - design of experiments: A key to innovation in nanotechnology, in: W. Ahmed, M.J. Jackson (Eds.), Emerging Nanotechnologies for Manufacturing, in: Micro and Nano Technologies, William Andrew Publishing, Boston, 2010, pp. 207–234, http://dx.doi.org/10.1016/B978-0-8155-1583-8.00008-9.

[35] S.C. Ferreira, R. Bruns, H.S. Ferreira, G.D. Matos, J. David, G. Brandão, E.P. da Silva, L. Portugal, P. Dos Reis, A. Souza, W. dos Santos, Box-Behnken design: An alternative for the optimization of analytical methods, Anal. Chim. Acta 597 (2) (2007) 179–186, http://dx.doi.org/10.1016/j.aca.2007.07.011.

[36] J. Wang, W. Wan, Experimental design methods for fermentative hydrogen production: a review, Int. J. Hydrog. Energy 34 (1) (2009) 235–244, http://dx.doi.org/10.1016/j.ijhydene.2008.10.008.

[37] S.-J. Reyes, L. Lemire, Y. Durocher, R. Voyer, O. Henry, P.L. Pham, Investigating the metabolic load of monoclonal antibody production conveyed to an inducible CHO cell line using a transfer-rate online monitoring system, J. Biotech. 399 (2025) 47–62, http://dx.doi.org/10.1016/j.jbiotec.2025.01.008.

[38] J. Schellenberg, T. Nagraik, O.J. Wohlenberg, S. Ruhl, J. Bahnemann, T. Scheper, D. Solle, Stress-induced increase of monoclonal antibody production in CHO cells, Eng. Life Sci. 22 (5) (2022) 427–436, http://dx.doi.org/10.1002/elsc.202100062.

[39] M. Mäkelä, Experimental design and response surface methodology in energy applications: A tutorial review, Energy Convers. Manage. 151 (2017) 630–640, http://dx.doi.org/10.1016/j.enconman.2017.09.021.

[40] K. Valgepea, K.Q. Loi, J.B. Behrendorff, R. de SP Lemgruber, M. Plan, M.P. Hodson, M. Köpke, L.K. Nielsen, E. Marcellin, Arginine deiminase pathway provides ATP and boosts growth of the gas-fermenting acetogen *Clostridium autoethanogenum*, Metab. Eng. 41 (2017) 202–211, http://dx.doi.org/10.1016/j.ymben.2017.04.007.

[41] H. Nagarajan, M. Sahin, J. Nogales, H. Latif, D.R. Lovley, A. Ebrahim, K. Zengler, Characterizing acetogenic metabolism using a genome-scale metabolic reconstruction of *Clostridium ljungdahlii*, Microb. Cell Factories 12 (2013) 1–13, http://dx.doi.org/10.1186/1475-2859-12-118.

[42] A. Ebrahim, J.A. Lerman, B.O. Palsson, D.R. Hyduke, COBRApy: constraints-based reconstruction and analysis for Python, BMC Syst. Biol. 7 (1) (2013) 74, http://dx.doi.org/10.1186/1752-0509-7-74.

[43] P.J. Gorter de Vries, V. Mol, N. Sonnenschein, T.Ø. Jensen, A.T. Nielsen, Probing efficient microbial CO2 utilisation through metabolic and process modelling, Microb. Biotechnol. 17 (2) (2024) e14414, http://dx.doi.org/10.1111/1751-7915.14414.

[44] E. Noor, H.S. Haraldsdóttir, R. Milo, R.M. Fleming, Consistent estimation of Gibbs energy using component contributions, PLoS Comput. Biol. 9 (7) (2013) e1003098, http://dx.doi.org/10.1371/journal.pcbi.1003098.

[45] Q. Mariën, A. Regueira, R. Ganigué, Steerable isobutyric and butyric acid production from CO_2 and $H_2$by *Clostridium luticellarii*, Microb. Biotechnol. 17 (1) (2024) e14321, http://dx.doi.org/10.1111/1751-7915.14321.

[46] P. Hu, S.H. Bowen, R.S. Lewis, A thermodynamic analysis of electron production during syngas fermentation, Bioresour. Technol. 102 (17) (2011) 8071–8076, http://dx.doi.org/10.1016/j.biortech.2011.05.080.

[47] R. Sander, Compilation of Henry's law constants (version 5.0.0) for water as solvent, Atmospheric Chem. Phys. 23 (19) (2023) 10901–12440, http://dx.doi.org/10.5194/acp-23-10901-2023.

[48] J. Martínez-Ruano, A. Suazo, F. Véliz, F. Otálora, R. Conejeros, E. González, G. Aroca, Electro-fermentation with clostridium autoethanogenum: Effect of pH and neutral red addition, Environ. Technol. Innov. 31 (2023) 103183, http://dx.doi.org/10.1016/j.eti.2023.103183.

[49] J. Abrini, H. Naveau, E.-J. Nyns, Clostridium autoethanogenum, sp. nov., an anaerobic bacterium that produces ethanol from carbon monoxide, Arch. Microbiol. 161 (4) (1994) 345–351, http://dx.doi.org/10.1007/BF00303591.

[50] K. Valgepea, R.d.P. Lemgruber, K. Meaghan, R.W. Palfreyman, T. Abdalla, B.D. Heijstra, J.B. Behrendorff, R. Tappel, M. Köpke, S.D. Simpson, L. Nielsen, E. Marcellin, Maintenance of ATP homeostasis triggers metabolic shifts in gas-fermenting acetogens, Cell Syst. 4 (5) (2017) 505–515, http://dx.doi.org/10.1016/j.cels.2017.04.008.

[51] L.A. de Lima, H. Ingelman, K. Brahmbhatt, K. Reinmets, C. Barry, A. Harris, E. Marcellin, M. Köpke, K. Valgepea, Faster growth enhances low carbon fuel and chemical production through gas fermentation, Front. Bioeng. Biotechnol. 10 (2022) 879578, http://dx.doi.org/10.3389/fbioe.2022.879578.

[52] L. Oliveira, A. Rückel, L. Nordgauer, P. Schlumprecht, E. Hutter, D. Weuster-Botz, Comparison of syngas-fermenting *clostridia* in stirred-tank bioreactors and the effects of varying syngas impurities, Microorganisms 10 (4) (2022) 681, http://dx.doi.org/10.3390/microorganisms10040681.

[53] A. Oppelt, A. Rückel, M. Rupp, D. Weuster-Botz, Mixotrophic syngas conversion enables the production of meso-2, 3-butanediol with *Clostridium autoethanogenum*, Fermentation 10 (2) (2024) 102, http://dx.doi.org/10.3390/fermentation10020102.

[54] H. Ingelman, J.K. Heffernan, A. Harris, S.D. Brown, K.M. Shaikh, A.Y. Saqib, M.J. Pinheiro, L.A. de Lima, K.R. Martinez, R.A. Gonzalez-Garcia, G. Hawkins, J. Daleiden, L. Tran, H. Zeleznik, R.O. Jensen, V. Reynoso, H. Schindel, J. Jänes, S.D. Simpson, M. Köpke, E. Marcellin, K. Valgepea, Autotrophic adaptive laboratory evolution of the acetogen *Clostridium autoethanogenum* delivers the gas-fermenting strain LAbrini with superior growth, products, and robustness, New Biotechnol. 83 (2024) 1–15, http://dx.doi.org/10.1016/j.nbt.2024.06.002.

[55] M.P. Elisiário, W. Van Hecke, H. De Wever, H. Noorman, A.J. Straathof, Acetic acid, growth rate, and mass transfer govern shifts in cometabolism of *Clostridium autoethanogenum*, Appl. Microbiol. Biotechnol. 107 (17) (2023) 5329–5340, http://dx.doi.org/10.1007/s00253-023-12670-6.

[56] S. Wang, H. Huang, J. Kahnt, A.P. Mueller, M. Köpke, R.K. Thauer, NADP-specific electron-bifurcating [FeFe]-hydrogenase in a functional complex with formate dehydrogenase in *Clostridium autoethanogenum* grown on CO, J. Bacteriol. 195 (19) (2013) 4373–4386, http://dx.doi.org/10.1128/JB.00678-13.

[57] H. Xu, C. Liang, Z. Yuan, J. Xu, Q. Hua, Y. Guo, A study of CO/syngas bioconversion by *Clostridium autoethanogenum* with a flexible gas-cultivation system, Enzym. Microb. Technol. 101 (2017) 24–29, http://dx.doi.org/10.1016/j.enzmictec.2017.03.002.

[58] A. Infantes, M. Kugel, K. Raffelt, A. Neumann, Side-by-side comparison of clean and biomass-derived, impurity-containing syngas as substrate for acetogenic fermentation with *Clostridium ljungdahlii*, Fermentation 6 (3) (2020) 84, http://dx.doi.org/10.3390/fermentation6030084.

[59] M.E. Davin, R.A. Thompson, R.J. Giannone, L.W. Mendelson, D.L. Carper, M.Z. Martin, M.E. Martin, N.L. Engle, T.J. Tschaplinski, S.D. Brown, R.L. Hettich, *Clostridium autoethanogenum alters* cofactor synthesis, redox metabolism, and lysine-acetylation in response to elevated H_2:CO feedstock ratios for enhancing carbon capture efficiency, Biotechnol. Biofuels Bioprod. 17 (1) (2024) 119, http://dx.doi.org/10.1186/s13068-024-02554-w.

[60] M.T. Allaart, C. Korkontzelos, D.Z. Sousa, R. Kleerebezem, A novel experimental method to determine substrate uptake kinetics of gaseous substrates applied to the carbon monoxide-fermenting *Clostridium autoethanogenum*, Biotechnol. Bioeng. 121 (4) (2024) 1324–1334, http://dx.doi.org/10.1002/bit.28652.

[61] M. Mohammadi, A.R. Mohamed, G.D. Najafpour, H. Younesi, M.H. Uzir, Kinetic studies on fermentative production of biofuel from synthesis gas using *Clostridium ljungdahlii*, Sci. World J. 2014 (1) (2014) 910590, http://dx.doi.org/10.1155/2014/910590.

[62] K. Valgepea, R. de Souza Pinto Lemgruber, T. Abdalla, S. Binos, N. Takemori, A. Takemori, Y. Tanaka, R. Tappel, M. Köpke, S.D. Simpson, L. Nielsen, E. Marcellin, H_2 drives metabolic rearrangements in gas-fermenting *Clostridium autoethanogenum*, Biotechnol. Biofuels 11 (2018) 1–15, http://dx.doi.org/10.1186/s13068-018-1052-9.

[63] J. Bertsch, V. Müller, Bioenergetic constraints for conversion of syngas to biofuels in acetogenic bacteria, Biotechnol. Biofuels 8 (2015) 1–12, http://dx.doi.org/10.1186/s13068-015-0393-x.

[64] Y. Ni, P.-L. Hagedoorn, J.-H. Xu, I.W. Arends, F. Hollmann, A biocatalytic hydrogenation of carboxylic acids, Chem. Commun. 48 (99) (2012) 12056–12058, http://dx.doi.org/10.1039/C2CC36479D.